Cracks detection using active modal damping and piezoelectric components

Baptiste Chomette, Amâncio Fernandes, Jean-Jacques Sinou

HAL Id: hal-00840749
https://hal.science/hal-00840749

Cracks detection using active modal damping and piezo-electric components

Authors:

B. Chomette[a,b,*], A. Fernandes[a,b], J-J. Sinou[c]

[a] CNRS, UMR 7190, Institut d'Alembert, F-75005 Paris, France

[b] UPMC Université Paris 06, UMR 7190, Institut d'Alembert, F-75005 Paris, France

[c] Laboratoire de Tribologie et Dynamique des Systèmes UMR-CNRS 5513, École Centrale de Lyon, F-69134 Ecully, France

Corresponding author: B. Chomette (baptiste.chomette@upmc.fr)

Abstract

The dynamics of a system and its safety can be considerably affected by the presence of cracks. Health monitoring strategies attract so a great deal of interest from industry. Cracks detection methods based on modal parameters variation are particularly efficient in the case of large cracks but are difficult to implement in the case of small cracks due to measurement difficulties in the case of small parameters variation. Therefore the present study proposes a new method to detect small cracks based on active modal damping and piezoelectric components. This method uses the active damping variation identificated with the Rational Fraction Polynomial algorithm as an indicator of cracks detection. The efficiency of the proposed method is demonstrated through numerical simulations corresponding to different crack depth and locations in the case of a finite element model of a clamped-clamped beam including four piezoelectric transducers.

1 Introduction

Cracks can considerably modify the dynamics of a system and affect system safety in several industrial applications. Crack modeling can be the first step of a health monitoring strategy. Cracks can be modelled using several approaches [14], for example reduction in element stiffness or pinned joint at crack location [19, 26]. Rigid finite element method can be used to model cracks with a set of spring-damping elements of variable stiffness as shown by Kulesza and Sawicki [20]. The approach can be first linear if the crack is supposed to be opened [12] and second non linear if the crack breathing is taken into account [2, 9, 24]. Christides and Barr [10] shown that cracks can be modelled using exponential stiffness reduction in the case of Euler Bernoulli beams. This model takes into account the second moment of area reduction induced by the crack. Sinha et al [31] proposed a simplified model for the location of cracks based on a triangular variation of the stiffness in beam structures using measured vibration data. This approach based on a local formulation of the flexibility permits particularly to include the crack model in a finite element model assuming that the stiffness reduction all fall within a single element.

One way to detect cracks on structures is to employ modal testing in which changes in modal parameters such as variations in frequencies and mode shapes are used to detect damage. A review based on the detection of structural damage through changes in frequencies was discussed by Salawu [28]. Moreover, Dilena and Morassi [11] proposed damage identification based on changes in the nodes of mode shapes. They demonstrated that appropriate use of resonances and antiresonances can be used to avoid the non-uniqueness of damage location for symmetrical beams. Faverjon and Sinou [12] demonstrated that it is possible to detect the number of cracks in a beam and estimate both crack positions and sizes despite the presence of noise levels. Cracks can also be detected using observer [30] or using non linear phenomena in the case of cracked beams submitted to forced vibrations [1] or in the case of cracked rotors [29].

Piezoelectric components are usually used in health monitoring systems coupling to active control strategies such as active collocated control [23], active modal control [7, 15] or passive strategies [4, 17]. These strategies can be used in complex applications such as curved panels in a car body as shown by Hurlebaus [18], using evaluated modal parameters [32] or in the case of 3D mechanical structures [16]. There are more various finite element approaches to model piezoelectric components, using 3D-solid elements, plate or beam elements. Benjeddou [5] proposed a review of the

different piezoelectric finite elements, solid, shell, plate and beam. Sadilek and Zemcik [27] proposed a one-dimensional beam element based on Euler-Bernoulli theory using a bilinear distribution of the electric field potential [13]. This model permits particularly to link one dimensional piezoelectric and cracks theory in order to develop health monitoring strategies.

In the case of controlled structures or smart-structures including actuators, sensors and control loop, cracks can considerably modify the dynamics of the controlled system. Chomette et al. [6] shown that active modal control based on Linear Quadratic Algorithm is highly sensitive to the variation of boundary conditions and thus to structure modification. They demonstrated that differences between the cracked structure and the modal model used in the controller based on the uncracked structure lead to control performance decrease. Chomette and Sinou [8] investigated the possibility of detecting transversal cracks in controlled truss structures using variation in the amplitude of the controlled system frequency response function and shown that the control performance variation can be an indicator of transversal crack detection.

Therefore the present study proposes a new method to detect small cracks based on piezoelectric components and active modal damping. Firstly the model of a cracked Euler-Bernoulli beam including piezoelectric elements is proposed. The main purpose of the control system is here to detect cracks. Consequently, the control algorithm is secondly designed in order to see small cracks. The novelty of the proposed strategy is to applied active control to monitor the structure behavior. Finally the efficiency of the proposed method is demonstrated through numerical simulations corresponding to different crack depths and locations in the case of the finite element model of a clamped-clamped beam including four piezoelectric transducers.

2 Finite element modeling

In this section the finite element modeling of a multi-cracked Euler Bernoulli beam including piezoelectric components is proposed. Firstly the crack modeling extended on several elements and the piezoelectric modeling are detailed. Secondly the finite element modeling of the complete structure including cracks and piezoelectric elements is proposed.

2.1 Crack modeling

Christides and Barr [10] shown that the effect of a crack in a continuous rectangular beam can be considered using an exponential variation of the flexural stiffness EI where E is the Young modulus and I the second moment of area. This stiffness reduction can be approximated by a triangular reduction for the cracked element as explained by Sinha et al. [31] in order to include the reduction in a finite element model. If the stiffness reduction extends over more than one element the proposed approach have to be extended on several elements as shown in Fig. 1. Thus the stiffness reduction can be written in local coordinates for the pth element of length ℓ_e

$$EI^{\pm}(x_e, p) = EI_0 \pm \frac{E(I_0 - I_c)}{\ell_c}(x_e + (p-1)\ell_e - x_c^{\pm}), \tag{1}$$

where E, b, e_p and I_0 are the Young modulus, the weigth, the depth and the second moment of area of the uncracked beam respectively. e_c and I_c are the crack depth and the second moment of area of the cracked beam respectively. $^+$ and $^-$ define the left and right part of the crack as shown in Fig. 1. x_c, x_c^+ and x_c^- are the crack location and the affected stiffness location in global coordinates respectively. The affected stiffness zone is defined so that

$$x_c^+ - x_c^- = 2\,\ell_c, \tag{2}$$

where $\ell_c = 1.5\,e_p$ is the length of the affected stiffness based on experimental data [14]. The stiffness matrices are obtained using the standard integration based on the variation in flexural rigidity $EI^{\pm}(x_e, p)$

$$\mathbf{K}_{e,crack}^{\pm} = \int_0^{\ell_e} EI^{\pm}(x_e, p)\,\mathbf{N}_e''^{\,T}(x_e)\,\mathbf{N}_e''(x_e)\,dx_e \tag{3}$$

where the shape functions $\mathbf{N}_e$ are those for a standard Euler-Bernoulli element beam. Finally, the element stiffness matrix including a crack can be written using the p parameter

$$\mathbf{K}_{e,crack}^{\pm} = \mathbf{K}_e - \mathbf{K}c_e^{\pm}(p), \tag{4}$$

with

$$\mathbf{K}c_e^{\pm}(p) = \pm \frac{E\ (I_0 - I_c)}{\ell_c} \begin{pmatrix} \frac{6\,(2X_c + \ell_e)}{\ell_e{}^3} & \frac{2\,(3X_c + 2\,\ell_e)}{\ell_e{}^2} & -\frac{6\,(2X_c + \ell_e)}{\ell_e{}^3} & \frac{2\,(3X_c + \ell_e)}{\ell_e{}^2} \\ \frac{2\,(3X_c + 2\,\ell_e)}{\ell_e{}^2} & \frac{(4X_c + 3\,\ell_e)}{\ell_e} & -\frac{2\,(3X_c + 2\,\ell_e)}{\ell_e{}^2} & \frac{(2X_c + \ell_e)}{\ell_e} \\ -\frac{6\,(2X_c + \ell_e)}{\ell_e{}^3} & -\frac{2\,(3X_c + 2\,\ell_e)}{\ell_e{}^2} & \frac{6\,(2X_c + \ell_e)}{\ell_e{}^3} & -\frac{2\,(3X_c + \ell_e)}{\ell_e{}^2} \\ \frac{2\,(3X_c + \ell_e)}{\ell_e{}^2} & \frac{(2X_c + \ell_e)}{\ell_e} & -\frac{2\,(3X_c + \ell_e)}{\ell_e{}^2} & \frac{(4X_c + \ell_e)}{\ell_e} \end{pmatrix} \quad (5)$$

where $X_c = x_c^{\pm} - p\,\ell_e$ and $-\mathbf{K}c_e^{\pm}(p)$ is the stiffness reduction induced by the crack on the pth element and $\mathbf{K}_e$ the element stiffness matrix of an uncracked element.

Using this modeling, crack location is independant of the mesh and the mesh size can be modified to take into account other physical coupling like electromechanical coupling using piezoelectric elements. Due to the detection method based on linear control, the crack is supposed to be open and the breathing crack is not taken into account.

[Fig. 1 about here.]

2.2   Piezoelectric finite element modeling

The finite element modeling of a structure including piezoelectric elements [5, 22, 27] can be written

$$\begin{cases} \mathbf{M}_{uu}\ddot{\mathbf{u}} + \mathbf{K}_{uu}^{cc}\mathbf{u} + \mathbf{K}_{u\phi}\boldsymbol{\phi} = \mathbf{F} \\ \mathbf{K}_{\phi u}\mathbf{u} + \mathbf{K}_{\phi\phi}\boldsymbol{\phi} = \mathbf{Q} \end{cases}, \quad (6)$$

where $\mathbf{M}_{uu}$, $\mathbf{K}_{uu}^{cc}$, $\mathbf{K}_{u\phi} = \mathbf{K}_{\phi u}^{T}$ and $\mathbf{K}_{\phi\phi}$ are the mass, the short-circuit stiffness, the electromechanical coupling and the dielectric matrix respectively. $\mathbf{u}$, $\boldsymbol{\phi}$, $\mathbf{F}$ and $\mathbf{Q}$ are the mechanical displacement vector and electrical potential, the force and the electrical charge vector respectively. The generalized electromechanical coupling coefficient k_ℓ is defined [17] for the ℓth mode as

$$k_\ell^2 = \frac{\omega_{co_\ell}^2 - \omega_{cc_\ell}^2}{\omega_{co_\ell}^2}, \quad (7)$$

where ω_{co_ℓ} and ω_{cc_ℓ} are the ℓth pulsations with open and short circuited electrodes respectively. The generalized electromechanical coupling coefficient is used to characterize piezoelectric actuators and sensors efficiency in the control algorithm.

5

2.3 Model of the complete beam

The finite element model of the complete beam including multi-cracks and piezoelectric elements permits to take into account cracks in the generalized electromechanical coupling coefficient. It can be written using equations (4) and (6)

$$
\begin{cases}
\mathbf{M}_{uu}\ddot{\mathbf{u}} + (\mathbf{K}_{uu}^{cc} - \mathbf{K}_{crack})\,\mathbf{u} + K_{u\phi}\boldsymbol{\phi} = \mathbf{F} \\
\mathbf{K}_{\phi u}\mathbf{u} + \mathbf{K}_{\phi\phi}\boldsymbol{\phi} = \mathbf{Q}
\end{cases}
, \tag{8}
$$

where $\mathbf{K}_{crack}$ is the crack stiffness matrix after assembling the different beam elements of stiffness $\mathbf{K}_{e,crack}^{\pm}$.

3 Modal Control

Modal control is usually applied to reduce structural vibration in targeting the control energy only on the modes of interest and permits to reduce the actuators and sensors number [15]. The control algorithm is designed here in order to detect small cracks. The Linear Quadratic Gaussian (LQG) algorithm is chosen in this application to target the control only on the mode of interest with the weighting matrix in order to see the modal influence of the cracks. The LQG algorithm is based on a linear model of the structure.

3.1 Linear system

The linear control [23] is based on a linear model which can be described in the state form by

$$
\begin{cases}
\dot{\mathbf{x}} = \mathbf{A}\mathbf{x} + \mathbf{B}\mathbf{u}^* + \mathbf{W}w \\
\mathbf{y} = \mathbf{C}\mathbf{x}
\end{cases}
, \quad \mathbf{u}^* = -\mathbf{G}\hat{\mathbf{x}}, \tag{9}
$$

where $\mathbf{A}$ is the dynamical system matrix, $\mathbf{B}$ and $\mathbf{C}$ are the actuator and sensor matrices respectively and $\mathbf{W}$ is the excitation matrix. $\mathbf{x}$ is the state vector in modal coordinates. $\mathbf{y} = {}^t(y_1 \ \ y_2)$ is the output vector detailed here in the case of two sensors. $\mathbf{u}^* = {}^t(u_1^* \ \ u_2^*)$ is the optimal control solution of the Linear Quadratic Regulator problem, detailed here in the case of two actuators and calculated using the estimated state $\hat{\mathbf{x}}$ and the gain matrix $\mathbf{G}$. w is the excitation applied on the beam and choosen to be unitary in this study. In practical applications, a white noise excitation can be applied using the piezoelectric actuators. The state matrices can be written for n modes, 2 actuators and 2

sensors

$$
\mathbf{A} = \begin{pmatrix} \mathbf{0}_{n,n} & \mathbf{Id}_{n,n} \\ -diag\left(\omega_\ell^2\right) & -diag\left(2\xi_\ell\omega_\ell\right) \end{pmatrix}, \mathbf{B} = \begin{pmatrix} \mathbf{0}_{n,1} & \mathbf{0}_{n,1} \\ \mathbf{\Pi}^{a_1} & \mathbf{\Pi}^{a_2} \end{pmatrix}, \mathbf{W} = \begin{pmatrix} \mathbf{0}_{n,1} \\ \mathbf{\Pi}^w \end{pmatrix}, \mathbf{C} = \begin{pmatrix} \mathbf{\Pi}^{c_1} & \mathbf{0}_{1,n} \\ \mathbf{\Pi}^{c_2} & \mathbf{0}_{1,n} \end{pmatrix}, \mathbf{x} = \begin{pmatrix} \mathbf{q} \\ \dot{\mathbf{q}} \end{pmatrix},
$$

$$(10)$$

with $\ell = \{1, n\}$, where $\mathbf{q}$ is the modal displacement vector, ω_ℓ and ξ_ℓ are the natural frequencies and damping respectively. $\mathbf{\Pi}^{a_i}$, $\mathbf{\Pi}^{c_i}$ and $\mathbf{\Pi}^w$ are the ith actuator, i^{th} sensor and disturbance vectors in the modal basis respectively ($i = \{1, 2\}$). In the case of piezoelectric actuators and sensors, the ℓth electromechanical coupling vector composants corresponding to the ith actuator can be written [6]

$$
\left(\Pi_\ell^{a_i}\right)^2 = \frac{\left(k_\ell^{a_i}\right)^2 C_p^{a_i} \left(\omega_{cc_\ell}\right)^2}{1 - \left(k_\ell^{a_i}\right)^2}, \tag{11}
$$

where ^{a} indicates actuator. k is the electromechanical coupling coefficient and C_p the piezoelectric component capacity. The piezoelectric component whose electromechanical coupling coefficient k is calculated using the equation (7), is modelled with open electrodes and all the other components are modelled with short circuited electrodes so that the only piezoelectric effect is due to the considered component.

3.2 Transfer functions in open and closed loop

The transfer function of the uncontrolled (open-loop) system $\mathbf{H}_{ol}$ can be written using equation (9) for one sensor of response y_1 as

$$
\mathbf{H}_{ol}\left(j\omega\right) = \frac{y_1}{w} = \mathbf{C}_s \left(j\omega\,\mathbf{Id} - \mathbf{A}_s\right)^{-1} \mathbf{W}_s, \tag{12}
$$

where $(\mathbf{A}_s, \mathbf{B}_s, \mathbf{C}_s, \mathbf{W}_s)$ is the state model that represents the structure in the numerical simulations. Frequencies and damping variation induced by the cracks are taken into account in the matrix $\mathbf{A}_s$. Mode shapes and electromechanical coupling coefficient variation induced by the cracks are taken into account in the $\mathbf{B}_s$, $\mathbf{C}_s$ and $\mathbf{W}_s$ matrices. The transfer function of the system controlled (closed-loop) $\mathbf{H}_{cl}$ can be written for one sensor as

$$
\mathbf{H}_{cl}\left(j\omega\right) = \frac{y_1}{w} = \mathbf{C}_s \left(j\omega\,\mathbf{Id} - \left(\mathbf{A}_s - \mathbf{B}_s\mathbf{G}\left(j\omega\,\mathbf{Id} - \left(\mathbf{A}_m - \mathbf{B}_m\mathbf{G} - \mathbf{L}\mathbf{C}_m\right)\right)^{-1}\mathbf{L}\mathbf{C}_s\right)\right)^{-1} \mathbf{W}_s, \tag{13}
$$

where $(\mathbf{A}_m, \mathbf{B}_m, \mathbf{C}_m)$ is the state model used by the Luenberger observer [21] to evaluate the state vector. $\mathbf{G}$ and $\mathbf{L}$ are the Linear Quadratic gain (LQ) and the observer gain of the Linear Quadratic Gaussian algorithm (LQG) [3] respectively.

3.3 Gain calculation to detect cracks

In the case of small cracks the frequency shift induced by the stiffness reduction cannot be easily measured. The proposed method consists in studying the dynamic of the closed loop system and to modify the control gain $\mathbf{G}$ in order to detect the cracks. The gain $\mathbf{G}$ is obtained using the quadratic criterion [23]

$$J = \int_0^\infty \mathbf{x}(t)^T \, \mathbf{Q} \, \mathbf{x}(t) dt \tag{14}$$

where $\mathbf{Q}$ is the classical weighting matrix. It can be written for n modes

$$\mathbf{Q} = \begin{pmatrix} \mathbf{Q}_{sup} & \mathbf{0}_{n,n} \\ \mathbf{0}_{n,n} & \mathbf{Q}_{inf} \end{pmatrix}. \tag{15}$$

The principle of the method is to design a little robust controller highly sensitive to the structure modifications. Therefore, the controller performance must be high and the robustness low. In this study, only the even modes are weighted using the $\mathbf{Q}$ matrix so that a frequency shift and an electromechanical coupling coefficient variation induce a slip of the controller effects on the even modes. In the case of uncracked structures only the weighted modes are highly actively damped using $\mathbf{Q}_{sup}$ and $\mathbf{Q}_{inf}$ and there is no effect on the odd modes. Weighting coefficient are arbitrarily chosen to target the control only on the wanted modes. In this study, three ponderations ($\mathbf{Q}_1$, $\mathbf{Q}_2$ and $\mathbf{Q}_3$) of the LQG controller are tested and the maximal weighting matrix $\mathbf{Q}_3$ is defined so that $\mathbf{Q}_{sup} = diag\,(1\ 1e15\ 1\ 1e17\ 1)$ and $\mathbf{Q}_{inf} = diag\,(1\ 1\ 1\ 1\ 1)$. In the case of cracked structures, the structural modifications induced by the cracks modify the controller dynamics and induce some active damping on the odd modes whereas the damping of the even modes decreases.

4   Numerical results

The clamped-clamped beam studied (length $L_p = 200\,mm$, thickness $e_p = 3\,mm$ and width $b_p = 20\,mm$) presented in Fig. 2 includes two piezoelectric actuators and two piezoelectric colocated sensors (length $L_{as} = 20\,mm$, thickness $e_{as} = 0.2\,mm$ and width $b_{as} = 20\,mm$) located closed to

8

the both clamping and made in PZT-5H whose mechanical and electromechanical properties can be found in table 1.

[Table 1 about here.]

Numerical simulations of section 4 are based on the open (without control) and closed (with control) loop transfer function between the excitation and the first piezoelectric sensor of the cracked structure. Modal parameters of the uncracked uncontrolled beam identified using the Rational Fraction Polynomial (RFP) algorithm [25] applied to the Frequency Response Function of the finite element model are detailed in table 2.

[Table 2 about here.]

Two crack location cases are studied to demonstrate the robustness of the detection method. In the first case three cracks are located on $x_{c_1} = 2.4$ mm, $x_{c_2} = 1\,mm$ and $x_{c_3} = 17.6\,mm$. In the second case two cracks are located at $x_{c_1} = 6\,mm$ and $x_{c_2} = 14\,mm$. The crack depth $\mu = \dfrac{e_c}{e_p}$ varies from 0 to $\dfrac{1}{4}$.

[Fig. 2 about here.]

The control loop presented in Fig. 3 includes a LQG controller based on a Luenberger observer. Frequency Response Functions (FRF) are measured between the excitation w and the first piezoelectric sensor. $\mathbf{u}^*$ is the optimal control calculated using the LQ gain $\mathbf{G}$, u_1^* and u_2^* are the control composants applied on the actuators 1 and 2. $\mathbf{y}$ is the output vector where y_1 and y_2 are the composants of the sensors 1 and 2. The model $(\mathbf{A}_s, \mathbf{B}_s, \mathbf{C}_s, \mathbf{W}_s)$ represents the multi-cracked beam including ten modes and $(\mathbf{A}_m, \mathbf{B}_m, \mathbf{C}_m)$ is the model of the uncracked structure including five modes used by the Luenberger observer to reconstruct the state vector $\hat{\mathbf{x}}$.

[Fig. 3 about here.]

The study focusses on the first fourth modes. Three ponderations ($\mathbf{Q}_1$, $\mathbf{Q}_2$ and $\mathbf{Q}_3$) of the LQG controller are tested in the two cases in order to show the proposed method efficiency, with $\mathbf{Q}_3 >> \mathbf{Q}_2 >> \mathbf{Q}_1$.

4.1   First case: three cracks

In this first case three cracks are located on $x_{c_1} = 2.4\,mm$, $x_{c_2} = 1\,mm$ and $x_{c_3} = 17.6\,mm$. A first study is carried out to show the influence of the crack depth on the electromechanical coupling

9

coefficient. Indeed, the piezoelectric actuators are here located in the section where the stiffness is affected by the first and fourth crack. This first study permits to know if the electromechanical coupling coefficient of the actuators and consequently the $\mathbf{B}_s$ and $\mathbf{C}_s$ matrices of the controller are affected or not. The coupling coefficient is calculated for several locations of one piezoelectric patch on the beam from $x_{as} = 0\,mm$ to $x_{as} = 180\,mm$, where x_{as} defines the left corner coordinate of the patch, and for a crack depth from $\mu = 0$ to $\mu = 1/4$. The evolution of the coupling coefficient is presented in Fig. 4(a) to 4(d). In these figures, the location of the piezoelectric component changes along the beam to look into all the sections of the structure where the stiffness is affected by the cracks. The excitation application point is constant. In the data shown in Fig. 5 to 8, the piezo-electric components and the force vector location are constants. There is a large variation of the coupling coefficient for the first and third mode when the patch is above the second crack. There is a large variation of the coupling coefficient for the fourth mode when the patch is above the first or third crack. There is a very small modification for the second mode. These modifications will be taken into account in the closed loop system dynamics calculation particularly in the $\mathbf{B}_s$ and $\mathbf{C}_s$ matrices which include the coupling coefficient. In closed loop, frequency and electromechanical coupling coefficient shift induce some differences between the state model of the controller and the real structure ($\mathbf{A}_s \neq \mathbf{A}_m$, $\mathbf{B}_s \neq \mathbf{B}_m$ and $\mathbf{C}_s \neq \mathbf{C}_m$). These differences can modify the closed loop structure dynamics and consequently induce some performance variations.

[Fig. 4 about here.]

Frequency response functions of the uncontrolled and controlled beam for three ponderations $\mathbf{Q}_1$, $\mathbf{Q}_2$ and $\mathbf{Q}_3$ are shown in Fig. 5(a), 5(b) and 5(c) for the first mode, in Fig. 5(d), 5(e) and 5(f) for the second mode, in Fig. 5(g), 5(h) and 5(i) for the third mode and in Fig. 5(j), 5(k) and 5(l) for the fourth mode. It can be observed that the presence of cracks decrease the frequencies of each mode. Moreover, increasing the crack size decrease modal frequencies. For the uncontrolled beam, the frequency variation induced by the crack depth variation from $\mu = 1/16$ to $\mu = 1/4$, usually measured to detect cracks, is about -0.8 to -3.8% for the first mode, 0 to -0.2% for the second mode, -0.5 to -2.3% for the third mode and -0.4 to -1.7% for the fourth mode. However, due to the small depth of each cracks, detection of the presence of cracks based on the evolution of natural frequencies appears to be not efficient. Identified frequency and damping for three weighting matrices are presented in Fig. 6(a), 6(b), 6(c) and 6(d) for the first fourth modes. The modal structural damping variation in less than 1% for the four modes. The damping variation for the

controlled beam using the $\mathbf{Q}_1$ weighting matrix is about 18.6 to 33.8% for the first mode and 7.6 to 12.6% for the third mode, 72 to 85% for the first mode and 51.1 to 65.9% for the third mode using the $\mathbf{Q}_2$ weighting matrix, 93.7 to 96.5% for the first mode and 81.0 to 91.9% for the third mode using the $\mathbf{Q}_3$ weighting matrix.

[Fig. 5 about here.]

[Fig. 6 about here.]

4.2   Second case: two cracks

In this second case two cracks are located at $x_{c_1} = 6\,mm$ and $x_{c_2} = 14\,mm$. Frequency response functions of the uncontrolled and controlled beam for three ponderations $\mathbf{Q}_1$, $\mathbf{Q}_2$ and $\mathbf{Q}_3$ are shown in Fig. 7(a), 7(b) and 7(c) for the first mode, in Fig. 7(d), 7(e) and 7(f) for the second mode, in the Fig. 7(g), 7(h) and 7(i) for the third mode and in Fig. 7(j), 7(k) and 7(l) for the fourth mode. There is the same decrease of the frequencies induced by the cracks depend on the crack depth. For the uncontrolled beam, the frequency variation induced by the crack depth variation from $\mu = 1/16$ to $\mu = 1/4$, usually measured to detect cracks, is about -0.1 to -0.5% for the first mode, -0.8 to -3.6% for the second mode, -0.3 to -1.4% for the third mode and -0.1 to -0.4% for the fourth mode. Consequently, the evolution of natural frequencies appears to be not efficient to detect cracks. Identified frequency and damping for three weighting matrices are presented in Fig. 8(a), 8(b), 8(c) and 8(d) for the first fourth modes. The modal structural damping variation in less than 2% for the four modes. The damping variation for the controlled beam using the $\mathbf{Q}_1$ weighting matrix is about 5.0 to 13.8% for the first mode and 5.2 to 13.5% for the third mode, 28.9 to 64.7% for the first mode and 38.6 to 64.3% for the third mode using the $\mathbf{Q}_2$ weighting matrix, 66.1 to 90.9% for the first mode and 68.7 to 90.7% for the third mode using the $\mathbf{Q}_3$ weighting matrix.

[Fig. 7 about here.]

[Fig. 8 about here.]

[Fig. 9 about here.]

The index variation is summarized in Fig. 9. The detection index based on frequency shift is calculated using the formula $100 \times \dfrac{f_{cracked} - f_{uncracked}}{f_{cracked}}$ and based on active modal damping using $100 \times \dfrac{\xi_{cracked} - \xi_{uncracked}}{\xi_{cracked}}$. Where ξ denotes the identified total damping, that is to say the structural

11

damping and the active damping whose variation is the most important. In the two cases, cracks induce a small frequency variation that cannot be experimentally measured and a very light structural damping variation. Using active damping, the damping variation is highly increased proportionally to the crack depth and induces a large amplitude variation of the controlled beam frequency response function that can be easily measured. The control is initially targeted on the second and third modes. The modal parameters variation, frequency shift, modal damping and mode shapes variation, induce some differences between the state model used by the controller and the real structure. These changes modify the controller behaviour and induce some active damping on the first and third modes initially very slightly controlled and are here used as an indicator of cracks presence. These results can be physically interpreted. The stiffness of the cracked structure is lower than the uncracked ones. The piezoelectric components are therefore more efficient and the electromechanical coupling coefficient is increased. This variation is taken into account in the $\mathbf{B}_s$ and $\mathbf{C}_s$ matrices. Moreover, the frequency shift included in the matrix $\mathbf{A}_s$ leads to disturb the modal control in the mode targeting. And as the control gains are not updated, the controller dynamics is changed. The proposed method is well adapted to detect small cracks increasing the weighting matrices and consequently the control voltage.

5   Conclusion

In this paper a new method to detect small cracks based on piezoelectric components and active modal damping is proposed. The originality of the proposed strategy is to exploit the fact that modal control is little robust. The main purpose of the control system is here to detect cracks. Consequently, the control algorithm is designed in order to detect cracks and the weighting matrix is chosen only to this task. Some weighting matrices can be tested by switching the controller between several values up to the crack detection. As the robustness of the controller is inversely proportional to the controller performances, the weighting coefficients must be increase in the case of small cracks. This method does not affect here the structure stability because the system is more and more damped. In other applications, the crack detection could induce some vibration amplification in state of damping but if the weighting matrices are tested increasingly, cracks must be detected before a too large amplification. Therefore, it can be applied to monitor the structure dynamics and to detect cracks instead of reduce vibration. The model of the uncracked structure, contained in the Luenberger observer permits to monitor the cracked structure dynamics. The main advantage of the use of a LQG controller to detect cracks is the possibility to use high control voltage

in the case of small crack depth when the frequency shift cannot be easily measured. The proposed method is validated with numerical simulation on a clamped-clamped cracked beam including four piezoelectric transducers linked by the LQG control loop. This approach could be extended to plates and more complex industrial systems. Weighting matrix coefficients could be optimize to detect small cracks using a minimum of energy. Moreover, the proposed method can be easily implemented with actuators and sensors traditionally used to detect cracks with frequency shift by adding a controller and an identification algorithm adapted to highly damped controlled systems.

References

[1] U. Andreaus, P. Baragatti, Experimental damage detection of cracked beams by using nonlinear characteristics of forced response, *Mechanical Systems and Signal Processing* **31** (2012), 382-404.

[2] M.A. Al-Shudeifat, E.A. Butcher, New breathing functions for the transverse breathing crack of the cracked rotor system: Approach and subcritical harmonic analysis, *Journal of Sound and Vibration* **31** (2011), 526-544.

[3] M. Athans, The role and use of the stochastic linear-quadratic-gaussian problem in control system design, *Automatic Control IEEE Transaction on* **16** (1971), 529-552.

[4] A. Badel, D. Guyomar, E. Lefeuvre, and C. Richard. Piezoelectric energy harvesting using a synchronized switch technique, *Journal of Intelligent Material and Structures* **17** (2006), 831-839.

[5] A. Benjeddou, Advances in piezoelectric finite element modeling of adaptive structural elements: a survey, *Computers and Structures* **76** (2000), 347-363.

[6] B. Chomette, D. Remond, S. Chesne, and L. Gaudiller, Semi-adaptive modal control of on-board electronic boards using identification method, *Smart Material and Structures* **17** (2008), 1-8.

[7] B. Chomette, S. Chesne, D. Remond, and L. Gaudiller, Damage reduction of on-board structures using piezoelectric components and active modal control - application to a printed circuit board, *Mechanical System and Signal Processing* **24** (2010), 390-397.

[8] B. Chomette and J-J. Sinou, Crack detection based on optimal control, *Journal of Vibration and Control* **18** (2012) 1737-1749.

[9] T.G. Chondros, Vibration of a beam with a breathing crack, *Journal of Sound and Vibration* **239** (2001), 57-67.

[10] S. Christides and A.D.S. Barr, One-dimensional theory of cracked Bernoulli-Euler beams, *International Journal of Mechanical Sciences* **26** (1984), 639-648.

[11] M. Dilena and A. Morassi, Identification of crack location in vibrating beams from changes in node positions, *Journal of Sound and Vibration* **255**(2002), 915-930.

[12] B. Faverjon and J-J. Sinou, Identification of an open crack in a beam by using a posteriori error estimator on the frequency response functions with noisy measurements, *European Journal of Mechanics A-Solid* **28** (2009), 75-85.

[13] A. Fernandes and J. Pouget. Analytical and numerical modelling of laminated composites with piezoelectric elements, *Journal of Intelligent Material Systems and Structures* **15** (2004), 753-761.

[14] M.I. Friswell and J.E.T. Penny, Crack modeling for structural health monitoring, *Structural Health Monitoring* **1** (2002), 139-148.

[15] L. Gaudiller and J. Der Hagopian, Active control of flexible structures using a minimum number of components, *Journal of Sound and Vibration* **193** (1996), 713-741.

[16] Z. Gosiewski, A.P. Koszewnik, Fast prototyping for the active vibration damping system of mechanical structures, *Mechanical Systems and Signal Processing* (2012), in press.

[17] N.W. Hagood and A. von Flotow, Damping of structural vibrations with piezoelectric materials and passive electrical networks, *Journal of Sound and Vibration* **146** (1991), 243-268.

[18] S. Hurlebaus, U. Stöbener, L. Gaul, Vibration reduction of curved panels by active modal control, *Computer and Structures* **86** (2008), 251-257.

[19] F. Ismail, A. Ibrahim, and H.R. Martin, Identification of fatigue cracks from vibration testing, *Journal of Sound and Vibration* **140** (1990), 305-317.

[20] Z. Kulesza, J. Sawicki, Rigid finite element model of a cracked rotor, *Journal of Sound and Vibration* **331** (2012), 4415-4169.

[21] D. Luenberger, An introduction to observers, *Automatic Control, IEEE Transactions on* **16** (1971), 596-602.

[22] V. Piefort, *Finite Element Modelling of Piezoelectric Active Structures*, Ph.D. Dissertation, Université libre de Bruxelles, 2001.

[23] A. Preumont, *Vibration Control of Active Structures: An introduction, second ed.*, Springer, 2002.

[24] N. Pugno and C. Surace, Evaluation of the non-linear dynamic response to harmonic excitation of a beam with several breathing cracks, *Journal of Sound and Vibration* **235** (2000), 749-762.

[25] H. Richardson, Mark and D.L. Formenti, Global curve fitting frequency response measurements using the rational fraction polynomial method, in *Proceeding of the International Modal Analysis Conference and Exhibit*, 1985, pp. 390-397.

[26] P.F. Rizos and N. Aspragathos, Identification of crack location and magnitude in a cantilever beam from the vibration modes, *Journal of Sound and Vibration* **183** (1990), 381-388.

[27] P. Sadilek and R. Zemcik, Frequency response analysis of hybrid piezoelectric cantilever beam, *Engineering Mechanics* **17** (2010):73-82.

[28] O.S. Salawu, Detection of structural damage through changes in frequency: a review, *Engineering Structures* **19** (1997), 718-723.

[29] J.T. Sawicki, M.I. Friswell, Z. Kulesza, A. Wroblewski, J.D. Lekki, Detecting cracked rotors using auxiliary harmonic excitation, *Journal of Sound and Vibration* **330** (2011), 1365-1381.

[30] J.T. Sawicki, Z. Kulesza, A new observer based method for rotor crack detection, *Advances in Vibration Engineering* **11** (2012), 131-141.

[31] J.K Sinha, M.I Friswell, and S. Edwards, Simplified models for the location of cracks in beam structures using measured vibration data, *Journal of Sound and Vibration* **251** (2002), 13-38.

[32] U. Stöbener, L. Gaul, Active vibration control of a car body based on experimentally evaluated modal parameters *Mechanical Systems and Signal Processing* **15** (2001), 173-188.

List of Figures

Fig. 1: Triangular stiffness reduction extended on several elements
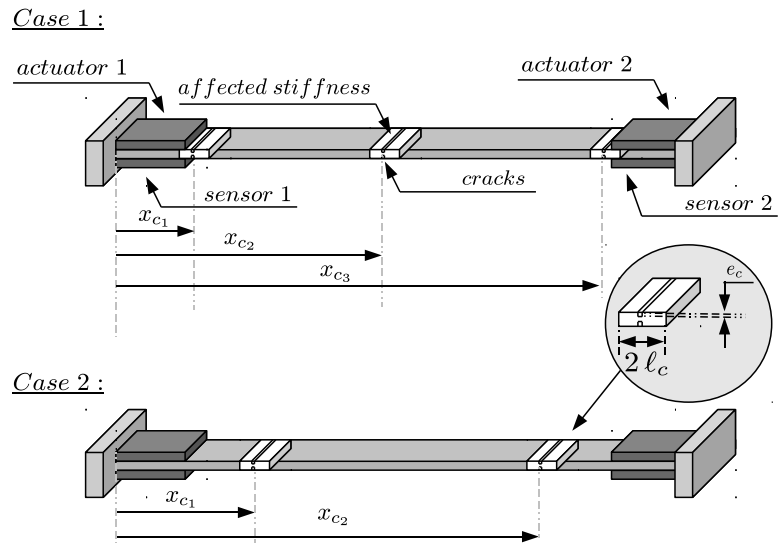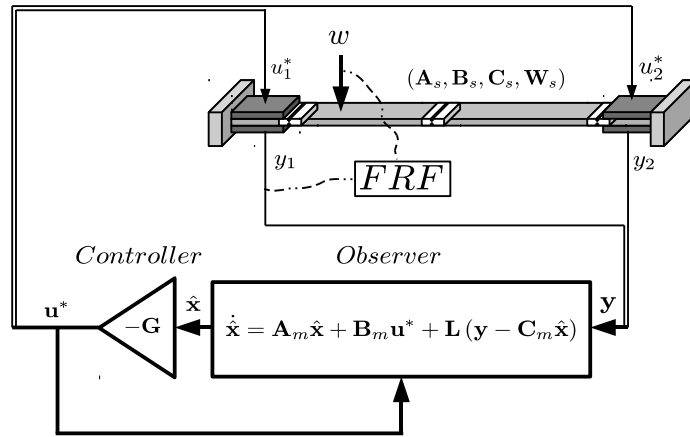
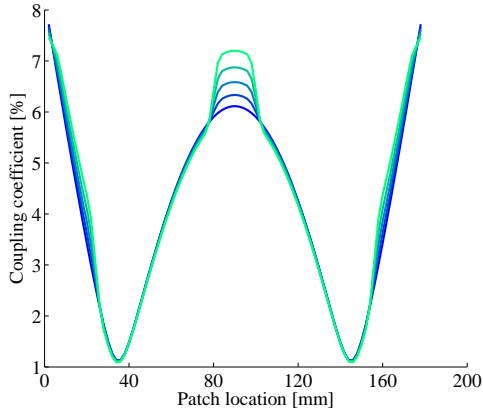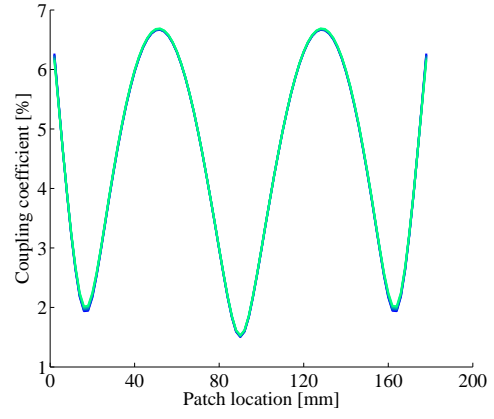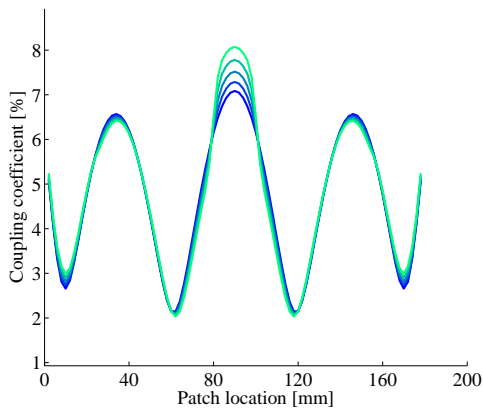Fig. 2: Multi-cracked composite beam in case 1 and 2

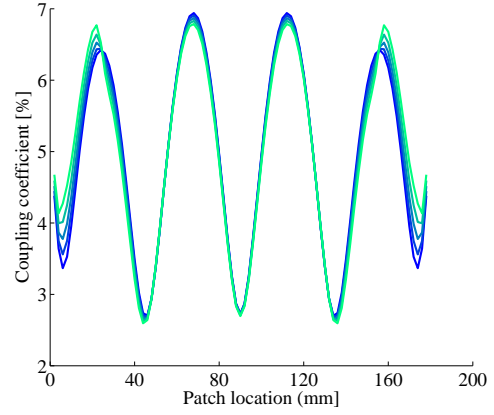Fig. 3: Controlled multi-cracked composite beam

(a) First mode

(b) Second mode

(c) Third mode

(d) Fourth mode

Fig. 4: Electromechanical coupling coefficient for one piezoelectric patch on the beam from $x_{as} = 0\,mm$ to $x_{as} = 180\,mm$ and for a crack depth from $\mu = 0$ to $\mu = 1/4$ (■: $\mu = 0$, ■: $\mu = 1/16$, ■: $\mu = 1/8$, ■: $\mu = 3/16$, ■: $\mu = 1/4$).
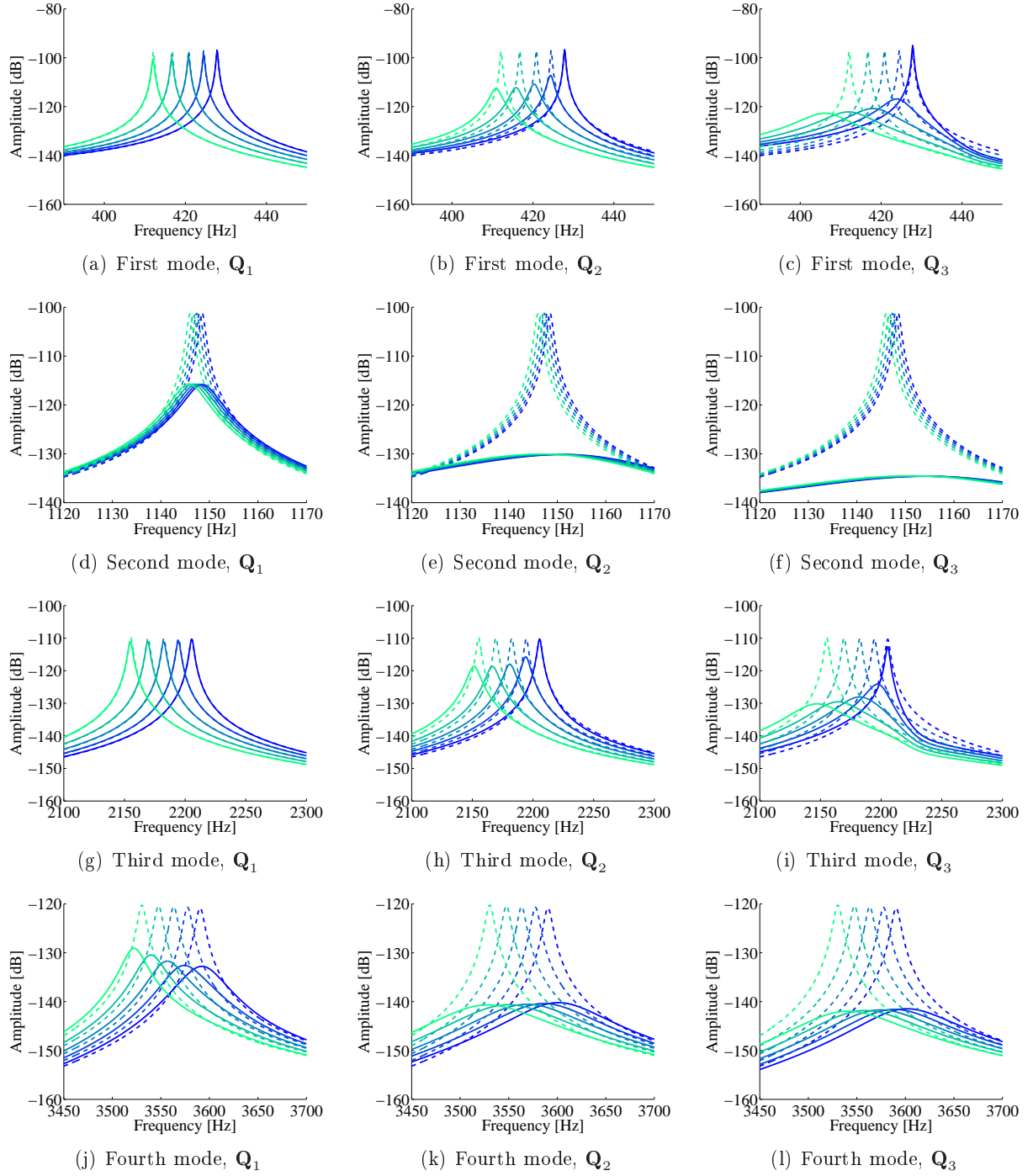
Fig. 5: Uncontrolled (- -) and controlled (——) FRF of the multi-cracked beam in the first case for the first fourth mode (■: $\mu = 0$, ■: $\mu = 1/16$, ■: $\mu = 1/8$, ■: $\mu = 3/16$, ■: $\mu = 1/4$) for three ponderations $\mathbf{Q}_1$, $\mathbf{Q}_2$ and $\mathbf{Q}_3$.
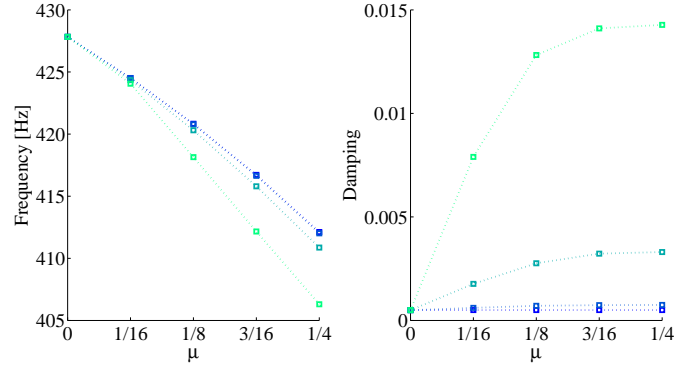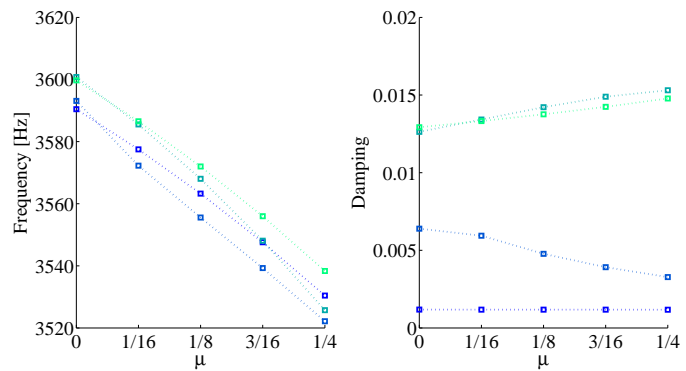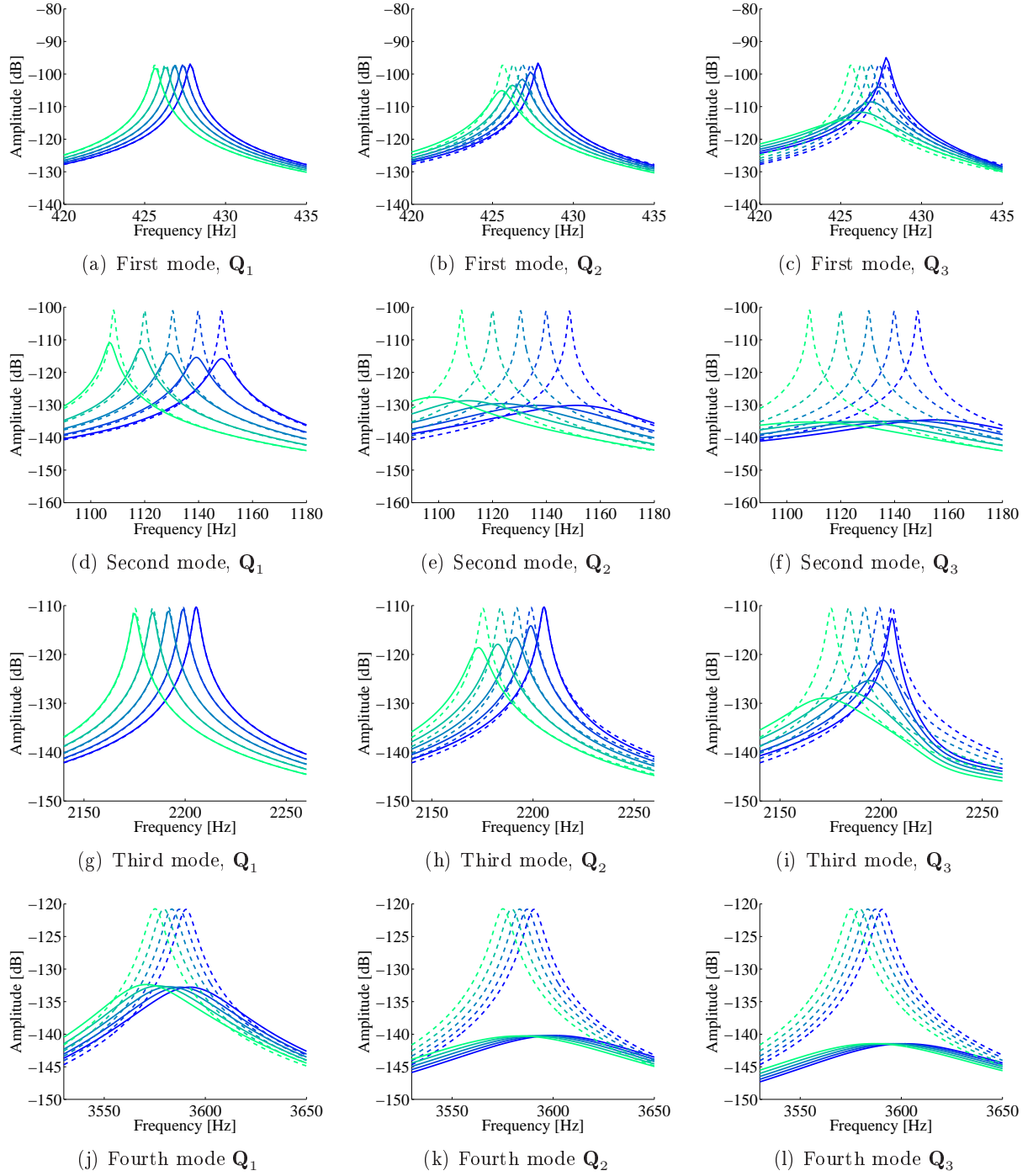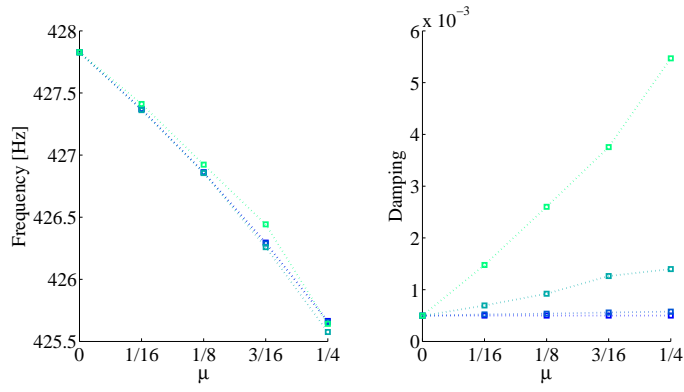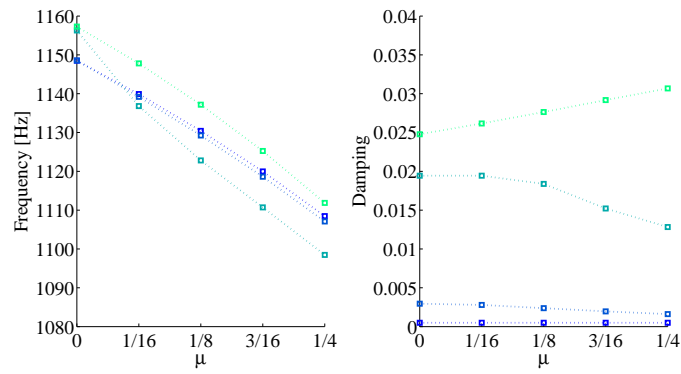
(a) First mode
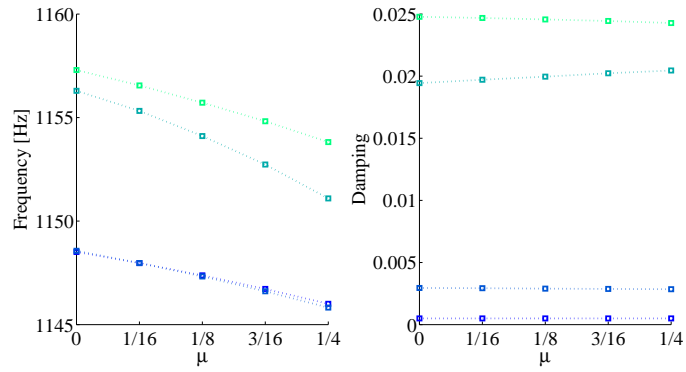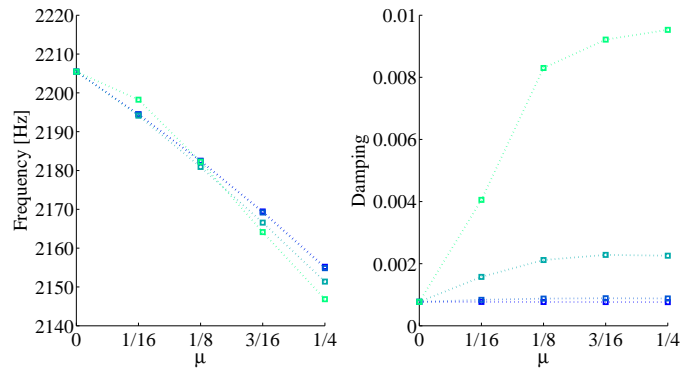
(b) Second mode

(c) Third mode

(d) Fourth mode

Fig. 6: Frequency and damping in the first case for three weighting matrices (■: uncontrolled, ■: $\mathbf{Q}_1$, ■: $\mathbf{Q}_2$, ■: $\mathbf{Q}_3$)

(a) First mode, $\mathbf{Q}_1$ (b) First mode, $\mathbf{Q}_2$ (c) First mode, $\mathbf{Q}_3$

(d) Second mode, $\mathbf{Q}_1$ (e) Second mode, $\mathbf{Q}_2$ (f) Second mode, $\mathbf{Q}_3$

(g) Third mode, $\mathbf{Q}_1$ (h) Third mode, $\mathbf{Q}_2$ (i) Third mode, $\mathbf{Q}_3$

(j) Fourth mode $\mathbf{Q}_1$ (k) Fourth mode $\mathbf{Q}_2$ (l) Fourth mode $\mathbf{Q}_3$

Fig. 7: Uncontrolled (- -) and controlled (—) FRF of the multi-cracked beam in the second case for the first fourth mode (■: $\mu = 0$, ■: $\mu = 1/16$, ■: $\mu = 1/8$, ■: $\mu = 3/16$, ■: $\mu = 1/4$) for three ponderations $\mathbf{Q}_1$, $\mathbf{Q}_2$ and $\mathbf{Q}_3$.
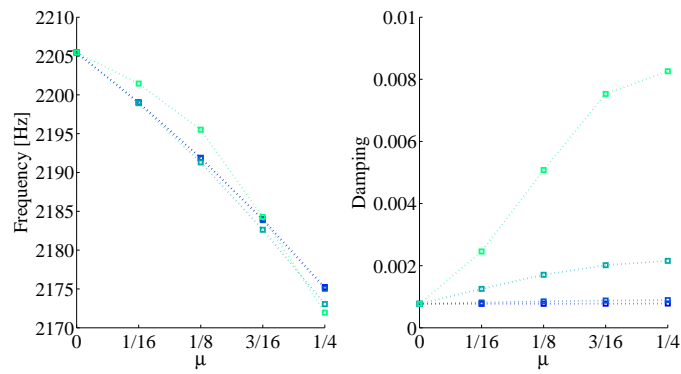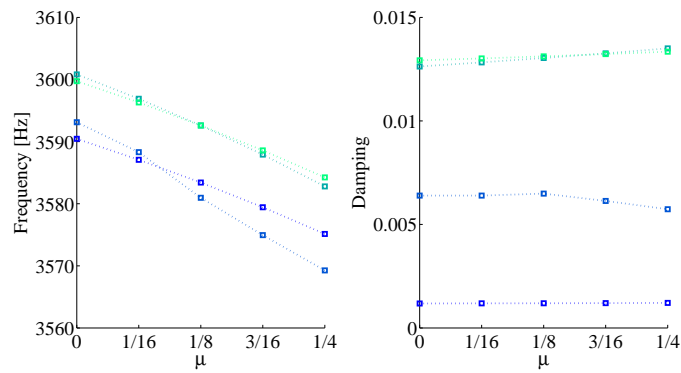
(a) First mode

(b) Second mode

(c) Third mode

(d) Fourth mode

Fig. 8: Frequency and damping in the second case for three weighting matrices (■: uncontrolled, ■: $\mathbf{Q}_1$, ■: $\mathbf{Q}_2$, ■: $\mathbf{Q}_3$)
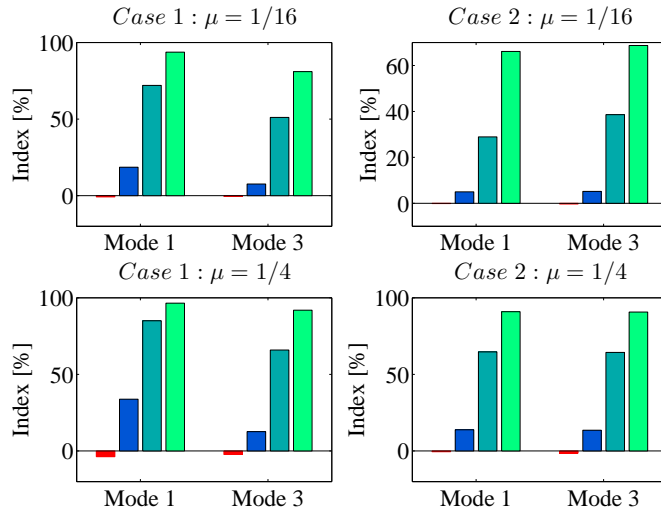
Fig. 9: Index variation in the first and second case for the first and third mode, calculated using frequency (■) or active damping for the three ponderations (■: Q_1, ■: Q_2, ■: Q_3) and two cracks depth ($\mu = 1/16$ and $\mu = 1/4$)

List of Tables

c_{11}^E (GPa)	c_{22}^E	c_{33}^E	c_{12}^E	c_{13}^E	e_{31} (C/m^2)	e_{33}	ϵ_{33}^S (nF/m)
127.2	127.2	117.4	802.1	846.7	-6.6	23.2	8.85

Table 1: Elastic, piezoelectric and dielectric constants of piezoelectric materials

Mode	Frequency [Hz]	Damping
1	427.8	5.00×10^{-4}
2	1148.5	5.00×10^{-4}
3	2205.5	7.70×10^{-4}
4	3590.4	1.18×10^{-3}

Table 2: Modal parameters of the uncracked uncontrolled beam